Research Article | Vol. 25, No. 26 | 25 Dec 2017 | OPTICS EXPRESS 33066
Optics EXPRESS

Solar rejection in laser based underwater communication systems

GIOVANNI GIULIANO,[1,2,*] LESLIE LAYCOCK,[2] DUNCAN ROWE,[2] AND ANTHONY E. KELLY[1]

[1] *School of Engineering, University of Glasgow, Glasgow, G12 8LT, UK*
[2] *BAE Systems Applied Intelligence, Great Baddow, Chelmsford, CM2 8HN, UK*
[*] *g.giuliano.1@research.gla.ac.uk*

Abstract: This article provides a numerical study of the expected improvements in an underwater optical system given by a single-mode laser diode operating within a Fraunhofer line in a coastal water type. The system performance is examined for a silicon PIN direct-detection receiver in the euphotic zone. The solar irradiance, modelled as white noise, is evaluated when using a lithium niobate interference and a birefringent filter with different field-of-view (FOV) characteristics in a clear sky situation. The results of this analysis show the inverse dependence of the signal-to-noise (SNR) on the FOV, along with the significant improvement in the receiver sensitivity given by a narrow optical bandpass filter (OBPF).

OCIS codes: (060.2605) Free-space optical communication, (010.4450) Oceanic optics, (140.7300) Visible lasers, (230.5160) Photodetectors, (230.7408) Wavelength filtering devices.

References and links

1. J. Bellingham, C. Goudey, T. Consi, J. Bales, D. Atwood, J. Leonard, and C. Chryssostomidis, "A second generation survey AUV," in *Proceedings of the 1994 Symposium on Autonomous Underwater Vehicle Technology* (IEEE, 1994), pp. 148–155.
2. B. Laval, J. S. Bird, and P. D. Helland, "An autonomous underwater vehicle for the study of small lakes," J. Atmos. Oceanic Tech. **17**, 69–76 (2000).
3. S. Watson, M. Tan, S. P. Najda, P. Perlin, M. Leszczynski, G. Targowski, S. Grzanka, and A. Kelly, "Visible light communications using a directly modulated 422 nm GaN laser diode," Opt. Lett. **38**, 3792–3794 (2013).
4. T. J. Slight, O. Odedina, W. Meredith, K. E. Docherty, and A.E. Kelly,"InGaN/GaN distributed feedback laser diodes with deeply etched sidewall gratings," IEEE Photonics Technology Letters **28**, 2886–2888 (2016).
5. M. A. Watson, P. M. Blanchard, C. Stace, P. K. Bhogul, H. J. White, A. E. Kelly, S. Watson, M. Valyrakis, S. P. Najda, L. Marona, and P. Perlin, "Assessment of laser tracking and data transfer for underwater optical communications," Proc. SPIE **9248**, 92480T (2014).
6. J. S. Cheong, J. S. L. Ong, J. S. Ng, A. B. Krysa, F. Bastiman, and J. P. R. David, "Design of high sensitivity detector for underwater communication system," Proc. SPIE **8899**, 88990G (2013).
7. S. Arnon, "Underwater optical wireless communication network," Opt. Eng. **49**, 015001 (2010).
8. G. C. Papageorgiou, and Govindjee, *Chlorophyll a Fluorescence: A Signature of Photosynthesis*, vol. 19 (Springer Science & Business Media, 2007).
9. M. Lovern, M. Roberts, S. Miller, and G. Kaye, "Oceanic in situ Fraunhofer-line characteristics (Fraunhofer-Line Underwater eXperiment: FLUX)", Tech. rep., DTIC Document (1992).
10. N. G. Jerlov, *Marine Optics* (Elsevier, 1976).
11. C. Mobley, "Light and Water: Radiative Transfer in Natural Waters" (Academic, 1994).
12. J. T. Kirk, *Light and Photosynthesis in Aquatic Ecosystems* (Cambridge University, 1994).
13. S. Koeppen and R. Walker, "Effective radiance attenuation coefficients for underwater imaging", in "19th Annual Technical Symposium," (International Society for Optics and Photonics, 1975), pp. 94–102.
14. X. Quan and E. S. Fry, "Empirical equation for the index of refraction of seawater," Appl. Opt. **34**, 3477–3480 (1995).
15. J. A. Simpson, B. L. Hughes, and J. F. Muth, "A spatial diversity system to measure optical fading in an underwater communications channel", in *IEEE OCEANS Conf., Biloxi, MS* (IEEE, 2009), pp. 1–6.
16. E. Hecht, *Optics* (Addison-Wesley, 2001).
17. A. Rabl, *Active Solar Collectors and Their Applications* (Oxford University, 1985).
18. M. Cvijetic, *Optical Transmission Systems Engineering* (Artech House, 2004).

#302936 https://doi.org/10.1364/OE.25.033066
Journal © 2017 Received 11 Oct 2017; revised 3 Dec 2017; accepted 4 Dec 2017; published 20 Dec 2017

Optics EXPRESS

19. R. Anderson and M. Hyde, "Underwater optical communications receivers", in *21st Annual Technical Symposium* (International Society for Optics and Photonics, 1978), pp. 79–88.
20. R. Hollins, A. Rudge, and S. Bennett, "Technologies for blue-green underwater optical communications," Proc. SPIE **8899**, 88990F (2013).
21. A. Title and W. Rosenberg, "Improvements in birefringent filters. 5: Field of view effects," Appl. Opt. **18**, 3443–3456 (1979).
22. E. Desurvire, *Classical and Quantum Information Theory: An Introduction for the Telecom Scientist* (Cambridge University, 2009).

1. Introduction

The growing number of human underwater activities, such as underwater sensor networks (UWSNs), remotely operated vehicles (ROVs) and autonomous underwater vehicles (AUVs), increases the need of efficient systems and devices for real-time monitoring and data transfer. Their use covers a wide range of applications, from difficult environments exploration (Arctic) [1] to small lakes [2]. One attractive option for underwater optical communications systems (UOCS) is underwater free-space optical (FSO) communication, a system that operates at transmission wavelengths matching the minimum absorption of water in the visible spectrum. This environment has widely varying optical properties, thus it represents one of the most complex and challenging modern engineering project. An UOCS has several advantages over traditional acoustic techniques: higher data rates and higher directionality, therefore low probability of detection (LPD) communications. Recent developments of high bandwidth (BW) GaN sources [3] and narrow single frequency laser with potentially high bandwidth [4] within the low loss transmission window of water in the blue-green region have heightened the need for a better understanding of UOCSs. The overall performances of an UOCS depend on the signal detected from a point optical source [5] and on the amount of sunlight that falls on the photodetector. In recent years, there has been an increasing interest in the development of high sensitivity photodetector in the blue-green wavelength range using alternative semiconductor materials to silicon, such as $Al_{0.52}In_{0.48}P$ homo-junction Separate-Absorption-Multiplication-Avalanche-Photodiode (SAM-APD) [6]. The reported full width at half maximum (FWHM) is narrower (22 nm) than a conventional silicon PIN and the responsivity can be as high as 25 A W^{-1}.

Different types of UOCS have been proposed along with the associated performance analyses: a line-of-sight (LOS), a modulating retroreflector (MRR) and a reflecting non-LOS (NLOS) [7]. LOS offers the highest data rate over a long range and the best power efficiency. Despite the potential advantage to overcome obstructions given by a NLOS reflecting system by using the reflection of the water surface, maintaining the link acquisition in such a system could be difficult due to the movement of water surface. Computer modelling is a fundamental tool in order to maximize the system performance by optimizing the spatial and temporal parameters. In this article, it is presented a model describing a one-way LOS link between a laser diode and a photoreceiver submerged up to a depth of 10 m in the context of applications with significant solar background. The analysis and modelling of operation within a Fraunhofer line is obtained with the development of a MATLAB source code. The model gives the possibility to simulate different scenarios and the effect of the various parameters on the overall system performance considering two filter technologies (interference and birefringent).

The model takes into account the individual noise terms (overall shot noise, thermal noise, background noise beat components) and outputs the signal-to-noise ratio (SNR) at the receiver, along with its sensitivity and response time, for a given field-of-view (FOV). These calculations are performed for a vertical link operating within the euphotic zone up to a depth of 10 m with both the transmitter and the receiver submerged, considering the latter pointing upwards in the direction of the water level. It is assumed that a tracking system is used in the system, *i.e.* the laser beam is aligned with the receiver so that the angle between the optical axis of the receiver and the LOS between them is zero. The importance of the inclusion of the solar background in the

Optics EXPRESS

system design, the resulting difference in two adjacent wavelengths and the necessary trade-off between SNR and FOV are drawn in Section (5).

2. The underwater light field

A solar spectrum with a subnanometer resolution exhibits many narrow dark lines that correspond to Fraunhofer lines. These narrow wavelengths intervals of relative intensity minima are a natural filters that represent absorption lines due to the cooler outer layers of the Sun's atmosphere containing vaporized elements. It is reasonable to expect that when the laser wavelength is operating within the FWHM of a Fraunhofer line, the sunlight background would be reduced. There are mainly three regions that are of interest to an UOCS: H-γ at 434.05 nm (FWHM = 0.35 nm); H-β at 486.143 nm (FWHM = 0.14 nm); Mg at 518.36 nm (FWHM = 0.16 nm) [8, 9]. At each of these wavelengths the solar irradiance is reduced with respect to the adjacent peak, hence also the background noise in an free-space optical (FSO) communication. Since the minimum value of the attenuation coefficient is shifting from blue wavelengths to green as the turbidity is increasing from clear ocean to harbour water [10], the optimum Fraunhofer line can be selected according to the water type.

In this context the results obtained from the latter are used and the simulations compare the overall performance of a system centered on the H-γ Fraunhofer line and one away from a Fraunhofer line at 490.220 nm while using the same bandwidth filter.

Considering an UOCS using a laser source with an initial power P_{LD} and a photodetector placed at a distance z, the transmitted optical power $P(z, \lambda)$ as a function of wavelength and distance is given by Beer's law [10, 11]

$$P(z, \lambda) = P_{LD} \exp(-c(\lambda) z) \tag{1}$$

The beam attenuation over the path length is given by the total extinction coefficient $c(\lambda)$, expressed as the sum of the absorption $a(\lambda)$ and scattering contributions: $c(\lambda) = a(\lambda) + b(\lambda)$ in units of m^{-1} of the aquatic medium. An additional present light field that has to be taken into account is the solar irradiance. The irradiance is the instantaneous density of solar radiation incident on the water surface [W m^{-2}], considering the sum of direct Sun radiation and the diffuse sky radiation. Due to the wavelength-selective attenuation mechanism, the blue and green ranges of the visible spectrum are the ones that can represent a source of interference in an UOCS even at a depth much greater than 10 m, depending on the extension of the euphotic zone.

Considering a monochromatic light, the irradiance decrease exponentially with depth and it is possible to write the dependence of spectral downward plane irradiance $E_d(z, \lambda)$ [W m^{-2}] as a function of its vertical attenuation coefficient K_d [m^{-1}] [10, 11]

$$E_d(z, \lambda) = E_d(0) \exp(-K_d(\lambda) z) \tag{2}$$

where $E_d(0)$ is the value of the downward irradiance just below the surface and the product is known as optical depth. Even if K_d depends on both the composition of the medium and directional structure of the light field, it has been shown that its values are mainly related to the inherent optical properties (IPOs) and not by the solar elevation [12]: smaller K_d values imply less attenuation as a function of depth, i.e. greater water clarity.

The clarity of different water types is classified into two categories, oceanic and coastal water. The former is subdivided into four categories (IA, IB, II, III) and the value of K_d at a specific wavelength is increasing from water type I to III. Similarly, coastal areas are classified into 1 to 9 categories, with an increasing value of turbidity and then also K_d. The present study considers a scenario in a coastal water type 1 that corresponds to a coastal area with low turbidity. The overall downward irradiance is a sum of different terms since the vertical attenuation coefficient is a function of the specific wavelength. In water types with a moderate turbidity, such as a coastal

Optics EXPRESS

area considered in this study, the downward irradiance attenuation coefficient has a value between the attenuation coefficient a and the total extinction coefficient c, depending on the amount of scattering b (Eq. (11c) in [13]). Following the previous optical water type classification, we used in our simulations a value of $K_d = 0.18\,m^{-1}$ that corresponds to a coastal area with low turbidity (Table XXVII in [10]).

The wavelength attenuation is higher in the red end of the visible spectrum and in the infrared region of the spectrum than in the blue-green range. Therefore, solar rejection is of the utmost importance for underwater free-space optical links operating close the water surface. As an example, the power associated with the solar irradiance in the range 280 nm to 1100 nm (power density of $710\,W\,m^{-2}$) for an unfiltered receiver with a squared active area of diameter $d = 0.01$ m placed just at the water surface is 71 mW. The impact of the background radiation is highly variable during the day and it depends on the link geometry. Then, the highest improvement is obtained when the receiver is most susceptible of the background light such as when facing upwards. It follows that it is important to minimise the interference by background sunlight in an UOCS, in particular when operating next the water level.

In order to estimate the refractive index of water, it is used the empirical Eq. given in [14]. It takes into account the variations of the water refractive index as a function of the salinity, temperature and wavelength at atmospheric pressure as a result of a polynomial containing 40 terms that reproduces the experimental data. The pressure changes are omitted but they can be neglected, as reported in [15] and because the system is simulated from the water level down to a depth of 10 m. At $\lambda_F = 486.143$ nm, with a temperature of 20 °C and a salinity of 3.5 % the calculated refractive index of seawater is $n_W = 1.3437$. A fraction of the incident light will be reflected at the interface water-filter due to the differing refractive indices between the two media. It can be estimated using Fresnel's Eqs., assuming a plane interface for the filter [16].

In the simulations, it is assumed a high transmission ($T_{LD} = 90\,\%$) for the filter/lenses in front of the laser and a relatively high transmission for the one in front of the receiver ($T_{RX} = 40\,\%$), both for an interference and a birefringent filter. The communication range can be extended by increasing the transmission power, using a laser beam with a small divergence ($\leqslant 1$ mrad) and using a receiver with a larger aperture. The latter, in the following simulations, is set to 10 mm.

3. Noise sources

In a real system various sources may cause an unwanted signal that is added to the measured one and these fluctuations from the ideal output voltage are classified as noise. This leads to errors in the conversion of the received signal and then limits the smallest signal that can be correctly read by the photodetector.

The upper limit of a silicon photodetector is limited to 1100 nm and then the solar irradiance is integrated over the range of wavelengths from 280 nm to 1100 nm. The incident direct solar radiation is modelled as having a random phase and polarisation, since the sunlight is unpolarised and the diffuse sky radiation has negligible effects on the polarisation [17].

The plots in Fig. 1 have been calculated for an intermediate depth of 5 m and a value of $K_d = 0.18\,m^{-1}$, as discussed above. The solar power density in the two top panels is obtained by integrating the solar irradiance over the range of wavelengths transmitted by the filter corresponding to the FOV reported on the x-axis. The same values (expressed in nm) are reported in x-axis of the two bottom panels. The power spectral density (PSD) is obtained by dividing the solar power density $E_d(z)$ by the filter bandwidth (expressed in Hz). The solar power density at a 5 m depth, $E_d(5m)$, in the 280 nm to 1100 nm range and without any filter is $126.8\,W\,m^{-2}$. Considering a the worst case scenario of an interference filter with a FOV = 60° (equivalent to a bandwidth of approximately 70 nm), the relative attenuation is −9.27 dB at both wavelength. For a birefringent filter with same FOV, the bandwidth drops to approximately 1.5 nm, thus the solar rejection is improved. In this case, the relative attenuation for a center wavelength

Optics EXPRESS

not corresponding to a Fraunhofer line (green continuous line in the plots) is −25.72 dB. This value is improved by operating within a Fraunhofer line (blue continuous line) since the relative attenuation in this case is −26.64 dB.

The differences between the two filters are due to the decreased angular dependence of a birefringent filter with respect to a conventional interference filter. This results in a wider FOV than the latter for the same solar background rejection. The plots in Figs. 1(c) and 1(d) indicate that the power spectral density (PSD) remains approximately constant across the frequencies transmitted through the narrow optical bandpass filter (OBPF) at a single wavelength. Hence it is reasonable to draw an analogy between background radiation and white noise which is treated with the traditional beat noise components in the amplifier analysis. The various sources of noise

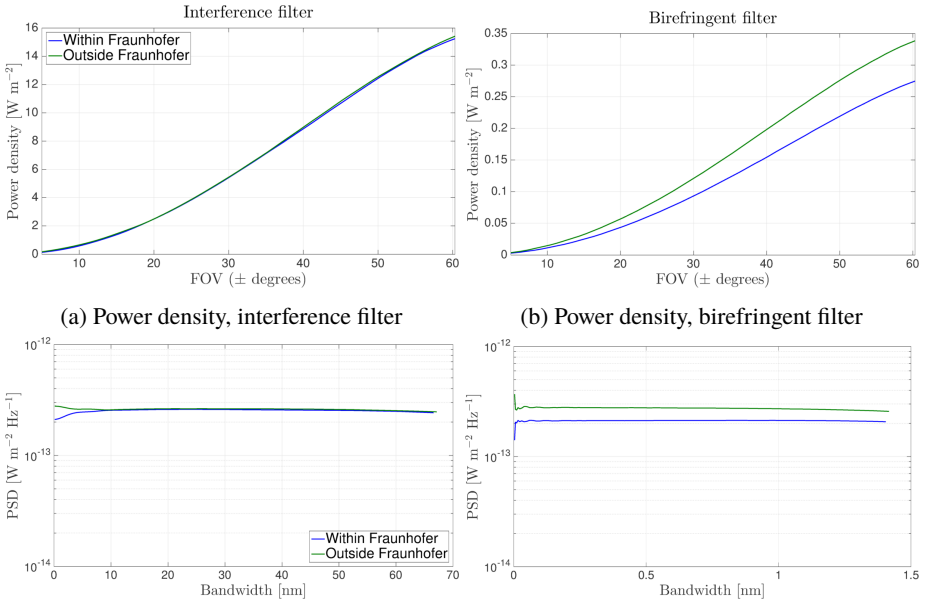

(a) Power density, interference filter

(b) Power density, birefringent filter

(c) Power spectral density, interference filter

(d) Power spectral density, birefringent filter

Fig. 1. (a)-(b) Solar background density density for two topologies of filter at a depth of 5 m. (c)-(d) Their relative PSDs are approximately constant for different filter bandwidths.

variance, expressed in A^2, are well known in the related literature [18, 19]. The overall shot noise includes also the dark current, I_D. Considering an incident optical signal with power P_{sig} and a background solar power P_{bg}, the shot noise variance at the receiver with a responsivity R, a gain M and a noise equivalent bandwidth BW_n is given by

$$\sigma_{sn}^2 = 2\,q\,M^2\,[R\,(P_{sig} + P_{bg}) + I_D]\,BW_n \tag{3}$$

The thermal (Johnson) noise, due to the resistive part of the input impedance R_L and the random thermal motion of electrons is given by

$$\sigma_{the}^2 = \frac{4k_B\,T\,BW_n}{R_L} \tag{4}$$

The impact of the thermal noise can be reduced by using a transimpedance amplifier (TIA), which has a load in the order of $k\Omega$. However, it is important to choose a TIA with an opportune bandwidth because it is limited to about $[2\pi RC]^{-1}$. Due to the incoherent nature of solar

Optics EXPRESS

background radiation, and following the analysis of the noise at the output of an optical amplifier, the total electric field at the detector is the sum of the fields from the background light and the signal light. The detector response is proportional to the square of the fields because there are two electrical beat-noise terms created: the signal-background beat noise σ^2_{sig-bg} and the background-background beat noise σ^2_{bg-bg}

$$\sigma^2_{sig-bg} = 4\,M\,R^2\,P_{sig}\,P_{bg}\,\frac{BW_n}{B_{op}} \tag{5}$$

$$\sigma^2_{bg-bg} = (R\,P_{bg})^2\left[2-\frac{BW_n}{B_{op}}\right]\frac{BW_n}{B_{op}} \tag{6}$$

where B_{op} is the optical filter bandwidth in [Hz].

Typical values for the main components of the numerical simulation of an UOCS are reported in Table (1). The signal levels for a digital transmission are characterized by average values I_1 and I_0, while the total noise is given by the sum of the standard deviations σ_1 and σ_0, that are given by the intensity of different noise components (Eqs. 3-(6)). The optical power incident on the receiver, taking into account the loss associated with filters and/or lenses in front of the transmitter T_{LD} and the receiver T_{RX}, is given by

$$P_1\,(x,\lambda) = T_{LD}\,T_{RX}\,P_{LD}\,\exp(-c\,(\lambda)\,z) \tag{7}$$

The power penalty necessary to reduce the rise time of laser pulses and its impact is described by the extinction ratio, given by the ratio of received optical powers associated with the 0 and 1 bit. Here it is assumed a non-zero value of $r_{ex} = P_0/P_1 = 0.1$, thus the noise terms related with the optical transmitted signal for the 0 bit are included in the model. Taking into account the non infinite value of the extinction ratio, the receiver sensitivity P_{rec} is defined as the minimum average power at the photoreceiver in order to reach a bit error ratio (BER) lower or equal to a specified value. The photocurrent associated with the two bits is given by $I_{(1,0)} = R\,P_{(1,0)}$. The resulting electrical SNR is defined as the ratio of the average signal power and the noise power, considering that the electrical power varies as the square of the current

$$SNR = \frac{(I_1-I_0)^2}{\sigma_1^2+\sigma_0^2} = \frac{[M\,R\,(P_1-P_0)]^2}{\sigma_1^2+\sigma_0^2} = \frac{[M\,R\,P_1\,(1-r_{ex})]^2}{\sigma_1^2+\sigma_0^2} \tag{8}$$

Various optical filter topologies exist which would represent feasible solutions for an UOCS operating within a Fraunhofer line. The more severe restriction results from its narrow FWHM (from 0.1 nm to 0.3 nm) compared to the detection range of a silicon photodetector (from 280 nm to 1100 nm). Then a narrowband filter matching this bandwidth and with a large extinction ratio (up to 40 dB) is referred to as Fraunhofer filter.

The FOV of an interference filter with a FWHM matching of a Fraunhofer line may be extremely narrow (< 2.5° [20]). Its value can be estimated from the angular dependence of the transmitted wavelength λ_{tr} expanded to second order in $\sin(\theta)$ (Eq. 7 in [21]). A conventional bandpass filter can be replaced by a Lyot or birefringent filter (BRF), that uses a linear arrangements of birefringent elements and linear polarisers to transmit a narrow range of wavelengths. The angular sensitivity of a BRF is described by (Eq. 18 in [21]). The previous Eqs. 3-(8) and analysis have been written in the MATLAB environment to simulate the system performance within and outside a Fraunhofer line. For each scenario, the resulting system performance given by two filters with typical specifications are evaluated.

4. Results

We consider the scenario of a laser source located at the water surface and pointing downward along the z axis where the upward-facing receiver is located. The simulations have been computed

Optics EXPRESS

Table 1. List of parameters used in this work for the simulated UOCS.

Transmitter		
Fraunhofer line, λ_F	486.143 nm	
Comparison line, λ_{out}	490.220 nm	
Laser power, P_{LD}	10 mW	
Beam radius, w_0	1.5 mm	
Full angular divergence, θ	1 mrad	
Extinction ratio, r_{ex}	0.1	
Filter/lenses transmittance, T_{LD}	90 %	
Medium		
Water type	Coastal, type 1	
Attenuation, c	0.4 m^{-1}	
Depth, z	0 m to 10 m	
Downward irradiance at water level, $E_d(0)$	710 W m^{-2}	
Vertical attenuation coefficient, K_d	0.18 m^{-1}	
Temperature, T	293.15 K	
Salinity, Sal	3.5 %	
Refractive index, n_w	1.3437	
Receiver		
Technology	Silicon PIN	
Gain, M	1	
Dark current, I_D	1 nA	
Unfiltered spectral range	280 nm to 1100 nm	
Electrical bandwidth, BW_n	1 GHz	
Responsivity, R	0.5 A W^{-1}	
Diameter, D	10 mm	
TIA load, R_L	1 kΩ	
Q-factor	6	
Filter type	**Interference**	**Birefringent**
Material	$LiNbO_3$, c_{Li} = 48.6 %	
Ordinary refractive index, n_o	2.3473	
Extraordinary refractive index, n_e	2.2523	
Filter/lenses transmittance, T_{RX}	40 %	
Optical bandwidth	0.14 nm to 77.20 nm	0.14 nm to 1.63 nm
FOV	2.3°−60°	16.0°−60°

for different angles of incidence and we compare the signal collected at several optical bandwidth (B_{op}) with the noise associated. At the water level, λ_F has a $FWHM$ = 0.14 nm [8, 9]. Then the maximum FOV that satisfies this narrow bandwidth is obtained considering two topologies of lithium niobate filters, using the aforementioned Eqs. [21]. The corresponding FOV is 2.3° for a conventional narrowband interference filter and 16.0° for a birefringent filter. For angles of incidence smaller than 16.0° the optical bandwidth is narrower than the Fraunhofer line when using a birefringent filter. The associated water level solar power densities E_0 at the two wavelengths chosen for the simulation, λ_F = 486.143 nm and λ_{out} = 490.220 nm, are respectively 0.157 W m^{-2} and 0.197 W m^{-2}, in the configuration of an optical filter with a $FWHM$ = 0.14 nm placed in front of the receiver. The scenario in which the system is operating within a Fraunhofer line without the use of a filter with a high spectral resolution is highly unlikely

Optics EXPRESS

due to its narrow FWHM. The advantage of using a narrow OBPF with a bandwidth of 0.14 nm is implemented in the next simulations, where the overall system performances are evaluated up to a depth of 10 m. It can be noticed that the background-background beat noise is independent

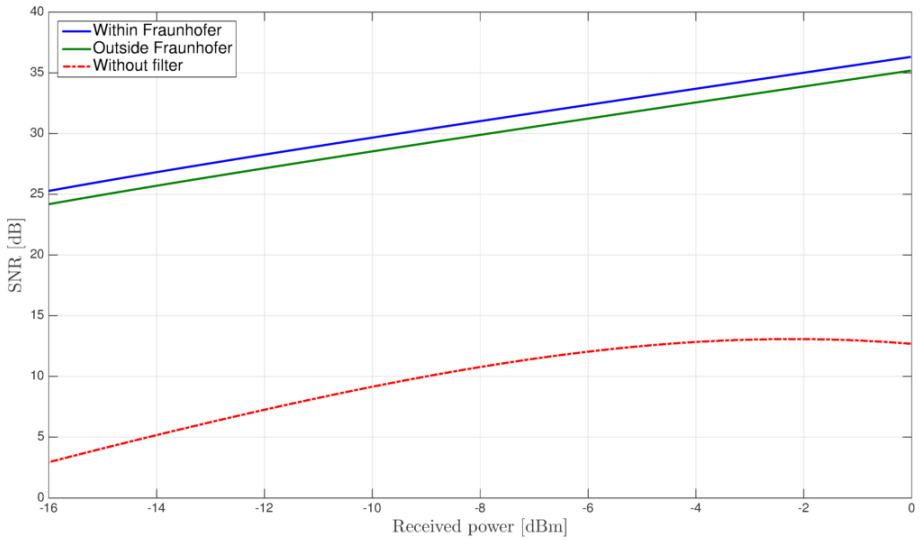

Fig. 2. Comparison of the electrical SNR as a function of the received power for a system within, outside a Fraunhofer line and for a receiver without any optical filtering.

of the input power in contrast with the other shot noises, such as the signal-background beat noise. In order to evaluate the effective impact in the noise components and then in the final SNR, these values are inserted into Equations (5) and (6). The resulting differences in the SNR profiles as a function of the received power are shown in Fig. 2. The thermal noise Equation (4) is reduced by using a large value of the high load resistance introduced by the TIA. It is worth noting that it has been assumed an OBPF, that has a relatively high transmittance ($T_{RX} = 40\,\%$) and in particular that it does not introduce any additional losses due to undesired wavelengths that are transmitted onto the detector active area. Another assumption that has been made is a perfect alignment between the transmitter and the receiver so that the laser beam reaching the receiver is collimated and entirely collected (*i.e.* an active laser pointing and tracking system). It can be noticed that there is a reduction in each of the noise components, as expected, thanks to the solar background rejection obtained by using a narrow OBPF. The dominant contribution to the photodetection noise comes from the signal-background beat noise A significant amount of noise power is caused also by the background-background beat noise, in particular when the receiver is next to the laser source, placed close to the water level. The inverse relation between the SNR and receiver FOV is investigated and shown in Fig. 3 for an arbitrary vertical distance between transmitter and receiver of 5 m. A system using a conventional PIN without any solar rejection in a sunny day and facing upwards would result in high levels of background noise. The practical negative effect of the different noise components is an increased power P_{rec} required to keep the specified BER. Under these circumstances, higher values are associated with longer communication range and when using a more conventional detector with a reduced or absent background rejection. It demonstrates that within a Fraunhofer line the solar background power is effectively reduced. In the PIN configuration, the reduced noise that reaches the receiver within a Fraunhofer line is translated into an average but not constant gain in the SNR of less than 1 dB, as plotted in Fig. 2. On the contrary, the higher solar background rejection of a birefringent filter is summarised in a gain up to 12 dB at both the optical wavelength. The larger collected background

Optics EXPRESS

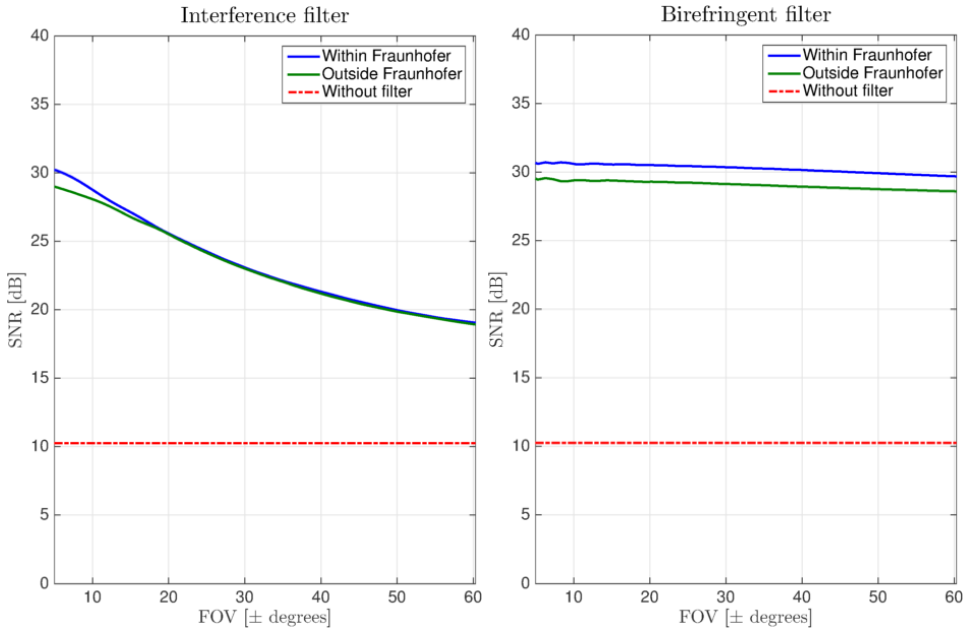

(a) Interference filter (b) Birefringent filter

Fig. 3. Comparison of the electrical SNR profiles as a function of the FOV at a depth of 5 m for various configurations at the receivers when adopting different filters.

intensity results in a SNR that tends faster to the plateau value corresponding to the scenario when no optical filter is placed in front of the receiver. A case study is presented for an UOCS with a system geometry given in Fig. 4 and with typical values reported in Table (1).

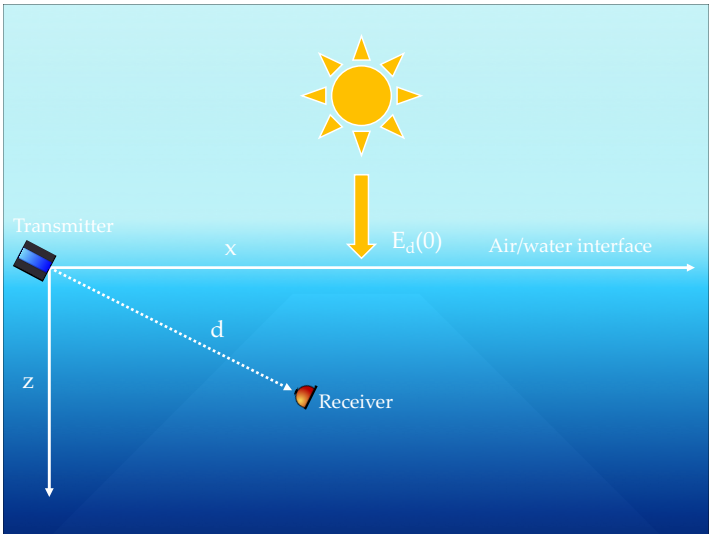

Fig. 4. Schematic of system geometry used in the simulations.

The results from the numerical simulation for different scenarios are shown in Fig. 5. The transmitter is located at the sea surface and the laser power is $P_0 = 10$ mW. The attenuation

Optics EXPRESS

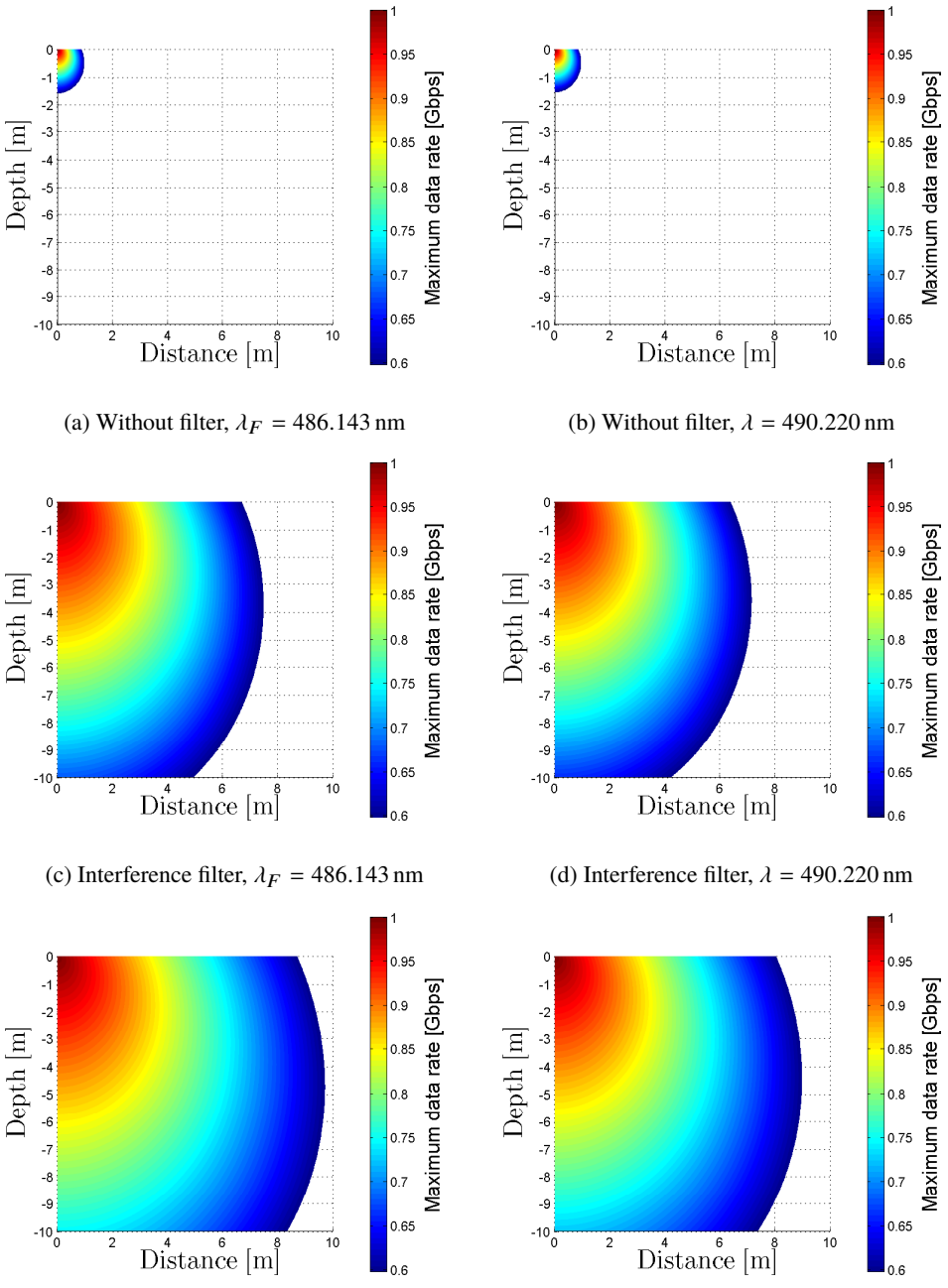

(a) Without filter, $\lambda_F = 486.143\,\text{nm}$

(b) Without filter, $\lambda = 490.220\,\text{nm}$

(c) Interference filter, $\lambda_F = 486.143\,\text{nm}$

(d) Interference filter, $\lambda = 490.220\,\text{nm}$

(e) Birefringent filter, $\lambda_F = 486.143\,\text{nm}$

(f) Birefringent filter, $\lambda = 490.220\,\text{nm}$

Fig. 5. Comparison of the maximum datarate for an UOCS operating at two different optical wavelengths without any optical filtering at the receiver, and with two different types of filter.

coefficient of seawater is $c = 0.4\,\text{m}^{-1}$ and its vertical attenuation coefficient $K_d = 0.18\,\text{m}^{-1}$, as discussed above. The upper limit on the data rate is set by the Shannon-Hartley theorem (excluding error-correction codes) depending upon the electrical bandwidth BW_n and the SNR

Optics EXPRESS

(expressed linearly) of the optical link

$$C = BW_n \, log_2 \, (1 + SNR) \, (bit/s) \tag{9}$$

over a square grid with sides 10 m long and step size of 1 mm. The modulation scheme implemented is a non-return-to-zero on-off-keying (NRZ-OOK), which has a maximum bandwidth efficiency of 1 bit/Hz which is achieved when SNR $\geq$ 5 dB [22]. The BER chosen is 1×10^{-9} and the required electrical SNR necessary to achieve error-free transmission is given by

$$BER_{NRZ-OOK} = \frac{1}{2} \, erfc \left(\frac{\sqrt{SNR}}{2\sqrt{2}} \right) \tag{10}$$

where *erfc* is the complementary error function. The active area diameter of the receiver is set to $d = 10$ mm, the electrical bandwidth is 1 GHz and it is assumed that the required FOV for an effective pointing and tracking system operation is $\pm 10°$. Combining the maximum data rate (1 bit per second) and the electrical bandwidth of the system, the theoretical maximum data rate is 1 Gbps. From the plots presented in Fig. 5, it is evident the advantage given by the implementation of an OBPF in an UOCS operating with solar background. Also, the reduced solar background within a Fraunhofer line gives no advantage in the system performance without a suitable matched filter at the receiver. The difference between Fig. 5(a) and Fig. 5(b) is negligible.

The difference between a transmission wavelength that matches a Fraunhofer line or not is less evident when using a narrowband interference filter with a FOV comparable with a BRF. This is because the range of wavelengths over which the solar irradiance is collected is much wider than the FWHM of the Fraunhofer line. In this scenario the wide FWHM of the interference filter reduces the solar rejection benefit of operating within a Fraunhofer line in the optical communication, as shown in Figs. 5(c) and 5(d). When comparing two filters for a given wavelength, the use of a BRF filter results in an increase of approximately 1 m in the vertical direction. Naturally, the range enhancement in the horizontal direction is higher (about 2 m), in particular when operating next to the sea surface where the solar background power is at its maximum. The scale of the colorbars in the six plots in Fig. 5 is kept constant for ease of comparison. The implementation of a BRF, in contrast with a interference filter, does not entail a degradation of the overall SNR even for wide FOV. In order to send more power at the receiver, which in turn will extend the communication range, a highly collimated beam and pointing accuracy are required in a laser based UOCS.

The use of a laser diode with a small divergence is beneficial for the system performance since it reduces the geometric loss giving the possibility to extend the communication range. The size of the collecting optics and the receiver aperture must be carefully taken into consideration in the system design process. A reduction in the receiver aperture entails an increased effect of the geometric loss and a more challenging tracking operation. On the other side, it also results in a reduced collection of the solar background radiation and in a shorter recharge time that would result in a higher bandwidth.

5. Conclusions

We have analysed the detrimental impact of the solar background power on the performance of an underwater optical communication system. When an optical filter is placed in front of the receiver, the PSD of the solar background over the range of transmitted wavelength can be treated as white noise. Hence, we have included in the overall SNR of the system also the amplifier equations with their associated traditional beat noise components. The results shown that it is the predominant source of noise, thus the main limiting factor. Based on standard solar irradiance data and parameters of silicon PIN direct-detection receiver, the SNR and FOV of the system have been analysed.

Optics EXPRESS

There is an improvement in the system performance as long as the bandpass filter has an optical bandwidth that is comparable to the Fraunhofer line's FWHM. When the range of wavelengths transmitted by the filter is much higher than the above FWHM, there is no practical advantage in operating within a Fraunhofer line. However, the performance improvement given by the implementation of an optical filter, either an interference or a birefringent one, is evident respect to the scenario where no filter is employed. This is due to the fact that the underwater link is operating near the sea level during the day, in a seawater with a relatively moderate turbidity. The decreased angular dependence of a birefringent filter spectral characteristic with respect to a conventional interference filter results in a wider FOV than the latter for the same solar background rejection. In this case, the use of a birefringent filter can give a gain up to 12 dB compared to a more conventional interference filter. The greater SNR produced is the result of the high solar light rejection that is translated into faster communications.

Collimated systems with active pointing and tracking laser system may use a conventional interference filter due to the narrow FOV. On the contrary, large FOV requirements would suggest the use of a BRF filter in front of the receiver. Also, for short range it may be adequate to use a relatively wide OBPF, whereas when using a narrow-linewidth single mode laser diode it requires a high spectral discrimination. In this work it has been considered only the optical attenuation due to the absorption, then increasing the laser power or the receiver sensitivity will result in a higher SNR. In the present study, the major system parameters have been chosen as indicative values and it is sensible to re-iterate the process to obtain a fine tuning and necessary design trade-off.

Funding

Engineering and Physical Sciences Research Council (EPSRC reference 1 566 934); BAE Systems Plc.